Redox-Dependent Conformational Selection in a $Cys_4Fe_2S_2$ Ferredoxin†

Thomas C. Pochapsky,*,‡ Milka Kostic,‡ Nitin Jain,‡,§ and Robert Pejchal||,⊥

Departments of Chemistry and Biochemistry, Brandeis University, Waltham, Massachusetts 02254-9110

Received December 19, 2000; Revised Manuscript Received March 15, 2001

ABSTRACT: Putidaredoxin (Pdx), a $Cys_4Fe_2S_2$ ferredoxin from *Pseudomonas putida*, exhibits redox-dependent binding to its physiological redox partner, cytochrome $P450_{cam}$ (CYP101), with the reduced form of Pdx (Pdx^r) binding with greater affinity to oxidized camphor-bound CYP101 than the oxidized form, Pdx^o. It has been previously shown that Pdx^o is more dynamic than Pdx^r on all accessible time scales, and it has been proposed that Pdx^r samples only a fraction of the conformational substates populated by Pdx^o on a time average. It is postulated that the ensemble subset populated by Pdx^r is the same subset that binds CYP101, providing a mechanism for coupling the Pdx oxidation state to binding affinity for CYP101. Evidence from a variety of sources, including redox-dependent shifts of ^{15}N and ^{13}C resonances, indicates that the metal cluster binding loop of Pdx is the primary determinant of redox-dependent conformational selection. Patterns of paramagnetic effects suggest that the metal cluster binding loop contracts around the metal cluster upon reduction, possibly due to the strengthening of hydrogen bonds between the sulfur atoms of the metal cluster and the surrounding polypeptide NH and OH groups. Effects of this perturbation are then transmitted mechanically to other affected regions of the protein. A specific mutation has been introduced into the metal binding loop of Pdx, G40N, that slows conformational exchange sufficiently that the ensemble of conformational substates in Pdx^o are directly observable as severe broadenings or splittings in affected NMR resonances. Many of the residues most affected by the mutation also show significant exchange contributions to ^{15}N T_2 relaxation in wild-type Pdx^o. As predicted, G40N Pdx^r shows a collapse of many of these multiplets and broadened lines to form much sharper resonances that are essentially identical to those observed in wild-type Pdx^r, indicating that Pdx^r occupies fewer conformational substates than does Pdx^o. This is the first direct observation of such redox-dependent ensembles at slow exchange on the chemical shift time scale. These results confirm that conformational selection within the Fe_2S_2 cluster binding loop is the primary source of redox-dependent changes in protein dynamics in Pdx.

The importance of protein dynamics in modulating protein function is now undisputed (*1*−*3*). We are particularly interested in the role that protein dynamics plays in modulating interactions between biological electron transfer partners. To that end, we are investigating the links between oxidation state, structure, and dynamics in the $Cys_4Fe_2S_2$ ferredoxin putidaredoxin (Pdx). Pdx is the physiological reductant and effector for cytochrome $P450_{cam}$ (CYP101).[1] CYP101 is the primary component of the camphor hydroxylase system from *Pseudomonas putida*, and catalyzes the 5-*exo*-hydroxylation of camphor by molecular oxygen in the first step in camphor metabolism by *P. putida*. The hydroxylation requires two electrons, which are shuttled sequentially from the NADH-dependent putidaredoxin reductase (PdR) to CYP101 by Pdx in two discrete events per turnover (for a review, see ref *4*). The interactions between Pdx and CYP101 are quite specific. CYP101 exhibits little or no cross reactivity with ferredoxins from homologous monooxygenase systems. Bovine adrenodoxin (Adx) is capable of transferring the first electron to CYP101, but substrate turnover is not observed in the camphor hydroxylase system reconstituted with Adx replacing Pdx (*5*). Even terpredoxin, a ferredoxin from another *Pseudomonas* monooxygenase enzyme system that is highly functionally and structurally homologous to Pdx, exhibits no more than 2% of the activity of Pdx in the reconstituted camphor monooxygenase system (H. Gong, unpublished results).

The reduced form of Pdx (Pdx^r) exhibits a binding constant for CYP101 that is 2 orders of magnitude greater than that

† This work was supported by a grant from the National Institutes of Health (RO1GM44191, to T.C.P.). R.P. gratefully acknowledges support from the Doris Brewer Cohen Fund (Brandeis University).

* To whom correspondence should be addressed: Department of Chemistry MS 015, Brandeis University, 415 South St., Waltham, MA 02454-9110. Phone: (781) 736-2559. Fax: (781) 736-2516. E-mail: pochapsk@brandeis.edu.

‡ Department of Chemistry.

§ Current address: CCRC, University of Georgia, Athens, GA 30602-4712.

|| Department of Biochemistry.

⊥ Current address: Department of Biochemistry, University of Michigan, Ann Arbor, MI 48109.

[1] Abbreviations: Adx, adrenodoxin; DTT, dithiothreitol; IPTG, isopropyl β-D-thiogalactoside; NMR, nuclear magnetic resonance; NOE, nuclear Overhauser effect; CYP101, cytochrome $P450_{cam}$; LB, Luria-Bertani medium; NOESY, NOE spectroscopy; HSQC, heteronuclear single-quantum correlation; MALDI-TOF, matrix-assisted laser desorption ionization time-of-flight; PdR, putidaredoxin reductase; Pdx^o, oxidized putidaredoxin; Pdx^r, reduced putidaredoxin; rms, root-mean-square; TPPI, time-proportional phase incrementation; WT, wild-type; 2D, two-dimensional; 3D, three-dimensional.

10.1021/bi0028845 CCC: $20.00
Published on Web 04/17/2001

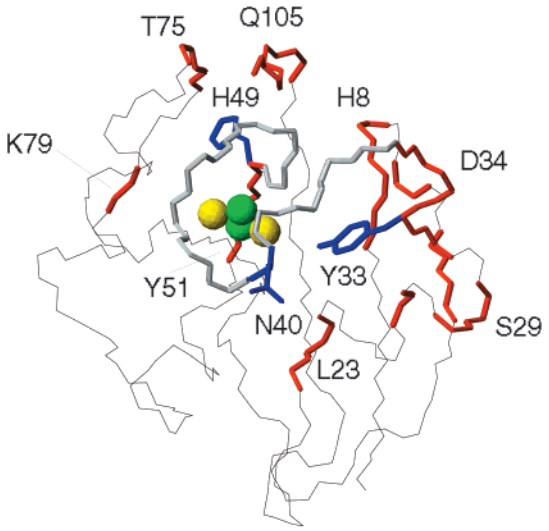

FIGURE 1: Backbone representation of the solution structure of oxidized Pdx as described in ref *10*. The orientation of the structure is approximately the same as in Figure 2 of ref *10*. The iron−sulfur cluster is shown as four spheres. Backbone positions marked in red are affected by the presence of the G40N mutation as shown in Figure 5. The backbone region shown in white is the metal cluster binding loop (Val 36−His 49), and is not directly observable in ^{1}H-detected NMR experiments. The side chains of Tyr 33 and His 49 are shown, as well as the expected location of the side chain of N40.

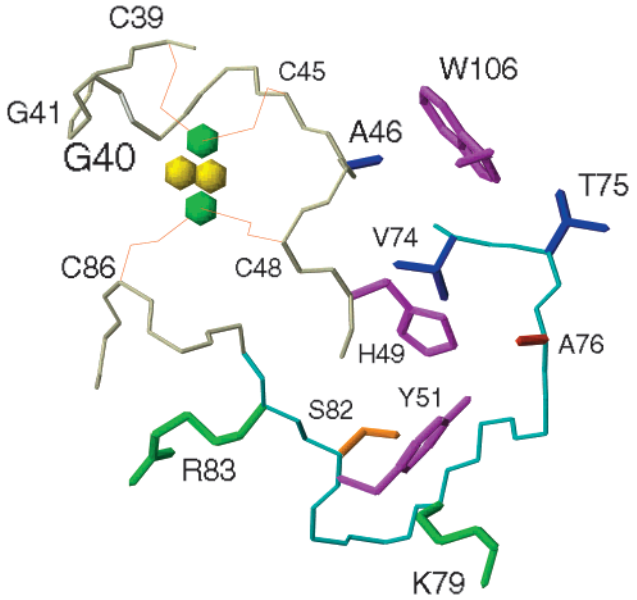

FIGURE 2: Fe_2S_2 binding loop and C-terminal cluster of Pdx from the structure in ref *10*. The region shown is approximately the top third of the structure shown in Figure 1, as viewed from the upper right of Figure 1. Residues His 49, Tyr 51, Ala 76, and Ser 82 are involved in the hydrogen bonding network proposed to transmit redox-dependent conformational changes from the metal cluster binding loop (backbone shown from Cys 39 to His 49) to the C-terminal cluster. Side chains of cysteinyl ligands to the metal cluster (Cys 39, Cys 45, Cys 48, and Cys 86) are shown as light lines.

of the oxidized form (Pdx^o) (*6*, *7*). This prevents product inhibition in the electron transfer between CYP101 and Pdx, a functionally important effect since two distinct binding and electron transfer events between the two proteins are required for each turnover of the CYP101 enzyme (*8*). Upon determining the structure of Pdx (*9*, *10*) (Figure 1), we began to examine redox-dependent differences between Pdx^o and Pdx^r as reflected by changes in ^{1}H chemical shifts and nuclear Overhauser effects (*11*). We found that the largest changes in the diamagnetic ^{1}H spectrum were observed in a region of the protein we termed the C-terminal cluster, which is formed by the interactions of a number of residues adjacent to the metal center. The C-terminal cluster includes the side chains of His 49, Tyr 51, Leu 71, Val 74, Thr 75, Ala 76, Leu 78, Lys 79, Ser 82, Pro 102, and Trp 106 (Figure 2). The largest diamagnetic ^{1}H and ^{15}N shift changes upon reduction of Pdx occur specifically at residues 49, 76, 77, and 106 (*12*). Trp 106 is the C-terminal residue of Pdx, and is critical for the binding interaction between Pdx and CYP101 (*13*). The indole ring of Trp 106 fits into a groove in the surface of Pdx between the methyl group of Ala 46 in the metal binding loop and Val 74 in the C-terminal cluster. We interpreted the spectral changes at Trp 106 in terms of an increased occupancy of the Trp 106 indole in this groove upon reduction (*11*). Other workers have noted redox-dependent changes in local dynamics for Trp 106 as well (*14*).

Later, we compared amide proton exchange rates as a function of oxidation state at the metal center (*12*). We found that, in general, Pdx^o was more dynamic than Pdx^r, with regions near the metal binding site and the C-terminal cluster being most affected. Sari et al. (*15*) examined the local dynamics of the diamagnetic regions of Pdx as a function of oxidation state using ^{15}N relaxation methods. They observed that order parameters for Pdx^r were generally higher than for Pdx^o, indicating more restricted motions of NH bonds in Pdx^r than in Pdx^o. The time scales measured by ^{15}N relaxation methods (picosecond to nanosecond) are shorter than those examined by amide exchange (millisecond to kilosecond). It is clear that Pdx dynamics exhibit similar redox effects over the whole range of experimentally accessible protein motions. Redox-dependent dynamic correlations have also been observed for cytochrome b_5 over a range of time scales (*16*).

Still, the mechanism by which the oxidation state of the Fe_2S_2 cluster affects local dynamics in Pdx remains unclear. Pdx^o appears to sample a larger conformational space on a time average than does Pdx^r. The potential energy surface traced by large-scale protein motions is rough, and can be envisioned as a series of substates that are separated by low potential barriers (*17*−*19*). We have postulated that Pdx^r occupies only a fraction of the substates occupied by Pdx^o (Figure 3), giving rise to smaller-amplitude motions in Pdx^r than in Pdx^o (*11*, *20*). On the basis of this model, we predicted that Pdx^o should be entropically favored relative to Pdx^r, and that this should lead to predictable temperature effects on the reduction potential of Pdx (*11*). The predicted temperature effects have now been observed experimentally by Vilker and co-workers (*21*).

Recently, we used selective ^{15}N and ^{13}C labeling combined with double-resonance techniques to assign most of the paramagnetically shifted and broadened amide ^{15}N and ^{13}C═O resonances in Pdx in the vicinity of the iron−sulfur cluster of Pdx in both oxidation states (*22*, *23*). Although our interpretation of these data is not yet complete, these assignments provide evidence for significant conformational differences in the metal binding loop of Pdx as a function of oxidation state (vide infra). On the basis of these data,

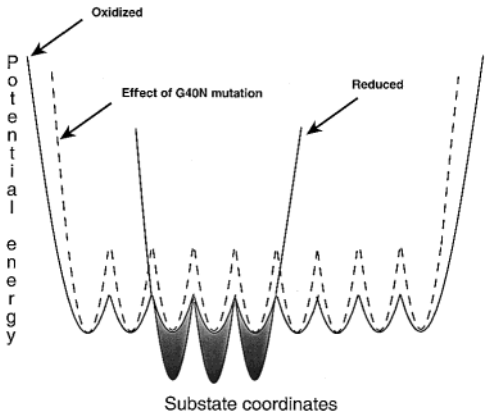

FIGURE 3: Simplified energy diagram illustrating proposed effects of redox-induced conformational selection in Pdx. The reduced form occupies a subset (highlighted by shading) of the conformations occupied by the oxidized form. The G40N mutation is proposed to raise the barriers between substates, slowing conformational interconversion. The figure is illustrative only; no real values for the energy differences are implied by the vertical axis, so it is unscaled.

we identified Gly 40 and Gly 41, two sequential glycine residues in the metal binding loop of Pdx, as potential hinges for multiresidue conformational fluctuations. We reasoned that, if we were to mutate those glycines to more conformationally restrictive residues, we might succeed in slowing exchange between conformational substates sufficiently to be able to detect those substates directly by NMR methods. We performed a series of site-directed mutagenesis experiments at residues 40 and 41, of which one mutation, G40N, achieved the desired slowing. We now report the results of these experiments.

MATERIALS AND METHODS

Site-Directed Mutagenesis and Plasmid Construction. The Pdx gene (*camB*) used for the current experiments was obtained from the plasmid pKM536, a pUC18-derived construct that places the *camB* gene under transcriptional control of the *lac* promoter, originally obtained from S. G. Sligar (University of Illinois, Urbana, IL). The *camB* clone in pKM536 contains significant 5′ and 3′ flanking regions that lack useful restriction sites. It was desirable to engineer restriction sites into the *camB* gene that simplified the use of the PCR (polymerase chain reaction) methodology in introducing mutations and permitting insertion of the gene into pET-derived vectors for improved expression. A four-primer mutagenesis method was used for introducing both the mutations and the restriction sites. This method uses two "side" primers and two "middle" mutagenic primers. The side primers introduce appropriate restriction sites at the 5′ and 3′ termini of the gene, and the middle primers introduce the desired mutation. Two separate PCRs are run in parallel. The first reaction is between the "left top" (5′) primer on the sense strand and the middle mutagenic primer on the antisense strand. The second reaction is between the "right bottom" (3′) primer on the antisense strand and the middle mutagenic primer on the sense strand. The products of the two reactions are two gene fragments. The first gene fragment contains an engineered restriction site, the start codon, and the 5′ end of the gene through the mutation site. The second fragment contains the mutation site through the 3′ end of the gene and an engineered restriction site following the stop codon. For the Pdx mutants described here, the left top primer includes an engineered *Nde*I restriction site as part of the initiating Met start codon. The right bottom primer contains an engineered *Bam*HI site. Care was taken in constructing the primers to ensure that there was enough DNA between the restriction site and the end of the primer (at least 5 bp) so that the restriction endonuclease was able to cut the DNA. Mutagenic primers were designed to melt at a temperature close to the melting point of the side primers, and were synthesized at the Brandeis University Oligonucleotide Synthesis Facility.

Primers for the mutations were as follows: Pdx side primers, 5′-GAGGATAAACATATGTCTAAAGTAGTG-3′ (T_m = 56.3 °C) and 5′-TTTTGGATCCCAGTGGTTTACC-ATT-3′ (T_m = 57.3 °C); Pdx mutagenic primers, 5′-TGA-TTGTGGCAGCGCCAGCTG-3′ (T_m = 61.7 °C) and 5′-CAGCTGGCGCTGCCACAATCA-3′ (T_m = 61.7 °C) for ΔG41, 5′-TGATTGTAACGGCAGCGCCAGCTG-3′ (T_m = 63.8 °C) and 5′-CAGCTGGCGCTGCCGTTACAATCA-3′ (T_m = 63.8 °C) for G40N, 5′-TGATTGTGGCAACAGCGC-CAGCTG-3′ (T_m = 63.8 °C) and 5′-CAGCTGGCGCTGT-TGCCACAATCA-3′ (T_m = 63.8 °C) for G41N, and 5′-TGATTGTAACAACAGCGCCAGCTG-3′ (T_m = 60.4 °C) and 5′-CAGCTGGCGCTGTTGTTACAATCA-3′ (T_m = 60.4 °C) for G40N/G41N.

PCRs for the four-primer method were performed in 29 steps, each step consisting of 1 min of denaturation (95 °C), 1 min of annealing (46 °C), and 1 min of extension (72 °C). Template (200 ng) and 50 pmol of each primer were used per reaction, combined with 1 μL of *Pfu* DNA polymerase (Stratagene), 10 μL of 10× *Pfu* buffer, 0.85 μL of dNTP (25 mM), 6 μL of 25 mM $MgCl_2$, and sufficient distilled water to give a total reaction volume of 100 μL. Upon completion, 20 μL of the parallel reaction mixtures was loaded on a 2% agarose electrophoresis gel; the product bands were identified by size and cut from the gel, and the DNA was extracted using a QIAGEN gel extraction kit. The two resulting gene fragments, one from each parallel PCR, were used as templates in a second PCR, in which they mutually prime each other and extend the gene to its full length. The complete Pdx gene containing the desired mutation was then amplified by a third PCR using the original side primers. After confirmation of the presence of the full-length gene product in the PCR mixture via gel electrophoresis, the product was isolated using the QIAGEN gel extraction kit and doubly digested with *Nde*I and *Bam*HI (NEB and Promega, respectively) for 24 h at 37 °C under a mineral oil cover layer. Expression plasmid pET23a(+) (Novagen) was digested in the polylinker region with *Nde*I and *Bam*HI under similar conditions. After purification, 50 fmol of doubly digested vector and 150 fmol of the doubly digested gene insert were mixed with 1.5 μL of T4 DNA ligase (NEB) and 1.5 μL of 20 mM ATP and diluted to a final volume of 30 μL in the appropriate buffer. The ligation was allowed to proceed for 16 h at 16 °C or for 24 h at 4 °C. Two microliters of the ligation mix was then added to a 50 μL suspension of electrocompetent XL1-Blue *Escherichia coli*, which were then transformed via electroporation. Five hundred microliters of cold LB was added to the transformed cells, and the cells were allowed to grow for 20 min at 37 °C prior to plating on agar containing appropriate nutrients and selective antibiotics. The entire length of the mutant gene

was sequenced using the dideoxy terminator method to confirm that the desired mutation was present and that no random mutations had been introduced.

Protein Expression, Reconstitution, and Purification. Wild-type and mutant Pdx were expressed in *E. coli* strain BL21-(DE3)pLysS by induction of T7 RNA polymerase production with IPTG. Bacteria were grown at 37 °C in LB supplemented with 200 μg/mL ampicillin (amp) (Sigma) and 34 μg/mL chloramphenicol (chl) (ICN). Electrocompetent BL21-(DE3)pLysS cells were transformed with the appropriate plasmid construct the day before growth and allowed to grow on chl- and amp-containing LB plates overnight. Separate colonies were used to inoculate 5 mL cultures in LB with amp and chl that were grown for 3.5 h and transferred to 50 mL of a minimal medium/amp/chl mixture. The 50 mL cultures were grown for an additional 2.4 h and transferred to 1 L of a minimal medium (M9)/amp/chl mixture. If ^{15}N-labeled samples were desired, the M9 was prepared containing 1 g of $^{15}NH_4Cl$ (CIL) as the sole nitrogen source. After the cultures reached an optical density of 1 at 600 nm, they were induced with IPTG (final concentration of 1 mM) and harvested after 8−12 h.

For most of the mutants, it was necessary to reconstitute the metal cluster into the protein after harvest. Only WT Pdx and G40N were expressed with an intact metal cluster, and even for these samples, reconstitution greatly improved yields. Reconstitution was achieved using a modified version of the protocol of Jain (*24*). Thirteen grams of cell paste was suspended in 39 mL of lysis buffer [66 mM Tris-HCl (pH 8.0), 1 mM DTT, 3.9 mg of DNAse 1, 2.9 mg of RNAse A, 104 mg of lysozyme, and 10 mg of tosyl chloride] and the mixture stirred overnight. The cells were cracked by sonication, and sufficient urea was added to the suspension with stirring under argon to reach a final urea concentration of 8 M. Sufficient DTT was added to reach a final concentration of 10 mM. After the mixture had been stirred under argon for 5 min, sufficient fresh $FeCl_2$ solution and Na_2S solution was added to reach a final concentration of 0.5 mM each. After being stirred for 10 min under argon, the solution was diluted 8-fold by adding 130 mL of degassed and argon-saturated 50 mM Tris-HCl (pH 7.4), followed by 160 mL of aerobically prepared 50 mM Tris-HCl (pH 7.4). The dilute solution was stirred under air for an additional 15 min, and then the pellets were removed by centrifugation. The cleared supernatant was then loaded onto a DEAE ion exchange column pre-equilibrated with 50 mM Tris-HCl (pH 7.4). A salt gradient (0.7 M KCl) was used to elute reconstituted ferredoxin from the column (elution occurs at ~0.4 M KCl). The purities of the eluted fractions were determined spectrophotometrically by measuring the A_{325}/A_{280} ratio. Fractions with ratios of >0.25 were collected, concentrated, and applied to a P30 (Bio-Rad) size exclusion column pre-equilibrated with N_2-sparged 50 mM Tris-HCl (pH 7.4) containing 1 mM DTT. Fractions from the P30 column with an A_{325}/A_{280} ratio of >0.66 were concentrated and buffer exchanged using a P2 (Bio-Rad) spin column pre-equilibrated with a 90/10 H_2O/D_2O mixture [20 mM *d*-Tris-HCl (pH 7.4) and 1 mM DTT]. Samples were typically 1−2 mM for NMR experiments. MALDI-TOF mass spectrometry was used to confirm the presence of the appropriate mutation. Mass spectra were obtained on a Perseptive Biosystems Voyager TOF mass spectrometer operating in the positive ion mode. Samples were desorbed from a sinapinic acid matrix. Calculated masses are 11 411 Da for WT Pdx, 11 470 Da for G40N and G41N Pdx, 11 354 Da for ΔG41 Pdx, and 11 527 Da for G40N/G41N Pdx. Observed masses were 11 413 Da for WT, 11 470 Da for G40N Pdx, 11 469 Da for G41N Pdx, 11 527 Da for G40N/G41N Pdx, and 11 355 Da for ΔG41 Pdx. Calculated mass differences between WT and mutants are as follows: G40N Pdx, 57 Da (57 Da observed); G41N Pdx, 57 Da (56 Da observed); G40N/G41N Pdx, 114 Da (112 Da observed); and ΔG41 Pdx, −57 Da (−56 Da observed).

Reduced Pdx samples were prepared in a Coy anaerobic chamber under a 5% H_2/95% N_2 atmosphere. Reduction was achieved by the addition of a small excess of a 1 M sodium dithionite solution that was freshly prepared in a degassed 1 M Tris-HCl buffer (pH 7.4). Upon reduction, the color of the protein changes from a chocolate brown to a clear ruby red, so the extent of reduction can be followed visually. After complete reduction, the sample was passed through a 1 mL spin column packed with P2 gel (Bio-Rad) that had been equilibrated with degassed 90% H_2O/10% D_2O [20 mM *d*-Tris-HCl (pH 7.4)] buffer. This effected buffer exchange and removal of excess dithionite and oxidation products of the reduction reaction.

Multidimensional NMR Experiments. Two-dimensional and three-dimensional NMR experiments were performed on either a Varian Unity Inova 500 11.74 T spectrometer or a Varian Unity Inova 600 14 T spectrometer. The Inova 500 operates at 499.709 and 50.641 MHz for ^{1}H and ^{15}N, respectively. The Inova 600 operates at 599.699 and 60.774 MHz for ^{1}H and ^{15}N, respectively. ^{1}H chemical shifts are referenced to external DSS using the ^{1}H resonance of H_2O as the internal reference. ^{15}N chemical shifts are referenced to external liquid ammonia using the ^{1}H resonance of H_2O as the internal reference (*25*). Coherence selection in all two- and three-dimensional experiments was achieved using pulsed field gradients, and sensitivity enhancement and phase sensitivity in the ^{15}N dimension was obtained using Rance-Kay acquisition and combinational processing schemes (*26*, *27*). GARP (*28*) composite pulse decoupling was used for broadband decoupling of ^{15}N during acquisition.

^{1}H−^{15}N HSQC, ^{15}N T_1, ^{15}N T_2, and three-dimensional ^{1}H−^{15}N NOESY-HSQC and ^{1}H−^{15}N TOCSY-HSQC experiments were performed on both the 500 and 600 MHz spectrometers (*27*, *29*, *30*). Unless otherwise noted, experiments were performed at 17 °C (290.15 K), with the ^{1}H carrier frequency of proton positioned at the water signal and carrier frequency of ^{15}N set at 118 ppm. Spectral widths of 8082 (11.74 T) and 10 000 Hz (14 T) were used for ^{1}H, and spectral widths of 1833.3 (11.74 T) and 3000 Hz (14 T) were used for ^{15}N. ^{15}N T_1 and T_2 experiments were carried out using 128 × 1024 complex points, with a total of 64 scans per t_1 point. To determine ^{15}N T_1 values, two separate runs were performed with variable delays (τ) of 20, 60, 200, 450, 700, and 950 ms and 40, 80, 250, 510, 750, and 1000 ms, respectively. For T_2 measurements, variable delays of both independent runs were 30, 50, 70, 90, 110, 150, 190, and 230 ms. To ensure complete recovery of the magnetization, delay times of 1.5 s were used between acquisitions. Protein concentrations of ~1 mM were used for ^{15}N

relaxation measurements for both Pdx^o and Pdx^r. The two-dimensional ^{1}H−^{15}N HSQC-NOESY experiment (*31*) was implemented for the Varian spectrometers by S. S. Pochapsky.

Relaxation data were processed using Felix, version 98.0 (Biosym Techologies, San Diego, CA), operating on a Silicon Graphics O_2 workstation. A Gaussian window function was applied in the directly detected dimension and a 90° shifted sine bell applied in the indirectly detected dimension. Peaks were identified on the basis of previously published assignments (*12*), and integrated peak volumes for 72 residues were determined from each data set. ^{15}N T_1 and T_2 values were extracted using a nonlinear least-squares curve fit of the integrated peak volumes as a function of delay time τ. The reported ^{15}N T_1 and T_2 values represent the average of two independent runs. For each residue, percentage errors for T_1 and T_2 represent the deviation between the experimentally determined results for two individual runs and the average reported. It was determined that for all residues, the percentage error does not exceed 2.5%.

RESULTS

Stability, Metal Cluster Incorporation, and Spectroscopic Characterization of Mutants. Of the mutations generated in Pdx for this study, only G40N spontaneously incorporates an iron−sulfur cluster in vivo. The other mutants (G41N, G40N/G41N, and ΔG41) are all expressed as apoproteins, and the efficiency and stability of Fe_2S_2 cluster incorporation of metal upon reconstitution vary from mutant to mutant. The UV−visible spectra of wild-type and G40N Pdx^o are essentially identical, with λ_{max} at 280, 325, 415, and 455 nm and similar extinction coefficients. In both the ΔG41 and G41N mutants, the 415 nm band red-shifts to ∼420 nm, and the 455 nm band broadens and loses significant intensity relative to the 415 nm band. Because of the relative instability of all of the mutants except for G40N, it was impractical to collect more than one-dimensional NMR spectra to characterize the reconstituted holoproteins. In all cases, it was clear from the 1D ^{1}H NMR spectra of the reconstituted ferredoxins that some folded structure was present after reconstitution. However, only in the case of the G40N mutant did we identify the downfield-shifted resonances of His 49 $N_{\delta 1}H$ and Ser 82 OH. Both of these protons are strongly hydrogen bonded in the C-terminal cluster of wild-type Pdx and provide useful markers for complete and stable folding in the C-terminal region of the protein.

Spectroscopic comparison of WT Pdx and G40N Pdx indicates that overall structural integrity is maintained in the mutant. Within experimental error, amide exchange rates in the slow exchange regime (which can be measured by the rate of H−D exchange on a time scale of hours to days) are the same in WT and G40N Pdx^o. The assignments of all resonances in the G40N mutant in both oxidation states were confirmed using data from 2D ^{1}H−^{15}N HSQC-NOESY and 3D ^{1}H−^{15}N NOESY-HSQC experiments. With the exception of the specific changes to be discussed below, there was no significant difference in chemical shift assignments for either oxidation state between WT and G40N Pdx. Observed NOE patterns are also very similar, indicating that there is no significant structural perturbation resulting from the G40N mutation.

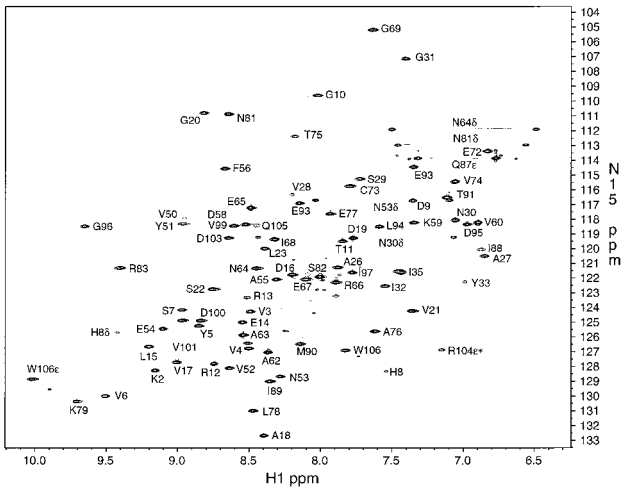

FIGURE 4: 14 T (600 MHz ^{1}H) ^{1}H−^{15}N HSQC spectrum of 1 mM WT Pdx^o at 290 K and pH 7.4 in 50 mM *d*-Tris-HCl buffer, with a 90/10 H_2O/D_2O mixture. The spectrum was obtained with maximum resolution in the ^{15}N dimension (complete ^{15}N decay envelope). The spectrum is plotted at a level sufficient to show most features without overlap. Resonances of D34 and R104 are observed, but only at contours lower than those plotted.

It is of interest to note that a new pair of ^{1}H−^{15}N correlations corresponding to the side chain NH_2 group of Asn 40 are observed in the HSQC spectrum of G40N Pdx in the region where the amide NH_2 groups of Asn and Gln are usually found. These represent the first diamagnetic resonances to be assigned for any residue in the metal cluster binding loop from Val 36 to Cys 48 of Pdx. It also indicates that the NMR-derived structural model of this region of the protein is correct insofar as it predicts that the side chain of a residue in position 40 should project away from the metal cluster (*10*). The same structure also predicts that non-glycine mutations at position 41 should interfere with the proper ligation of the metal cluster because the side chain of residue 41 would project into the metal cluster binding site. Poor in vivo incorporation of the metal cluster and low stability exhibited by the G41N and G40N/G41N mutants are thus also rationalized by the structural model.

Comparison of WT and G40N Pdx ^{1}H−^{15}N HSQC Spectral Maps. Although Pdx^o has a diamagnetic ground state, thermal population of unpaired spin states results in significant paramagnetic bleaching of the NMR spectrum of WT Pdx^o (Figure 4), including the loss of all backbone NH correlations for residues 24, 36−49, and 84−87. Several more NH correlations are lost in WT Pdx^r, which has a paramagnetic electronic ground state, including those of Leu 23, Val 50, Met 70, Leu 71, Arg 83, and Ile 88 (*12*). Patterns of paramagnetic broadening observed in both oxidation states of G40N Pdx are identical with those observed in WT Pdx (see Figure 5).

The primary differences between WT and G40N Pdx are found in the ^{1}H−^{15}N HSQC spectra of the oxidized forms. Figure 5 shows the ^{1}H−^{15}N HSQC spectra of G40N Pdx^o and of G40N Pdx^r. Positions marked by boxes on the two-dimensional spectra indicate positions of residues that are significantly perturbed between the WT and G40N Pdx^o spectra, but are comparable in intensity and line width in the WT and G40N Pdx^r spectra. Differences between WT and G40N Pdx^o are observed at the NH correlations of Val 6, Ser 7, His 8, Gly 10, Arg 12, Arg 13, Ala 27, Ser 29, Asn

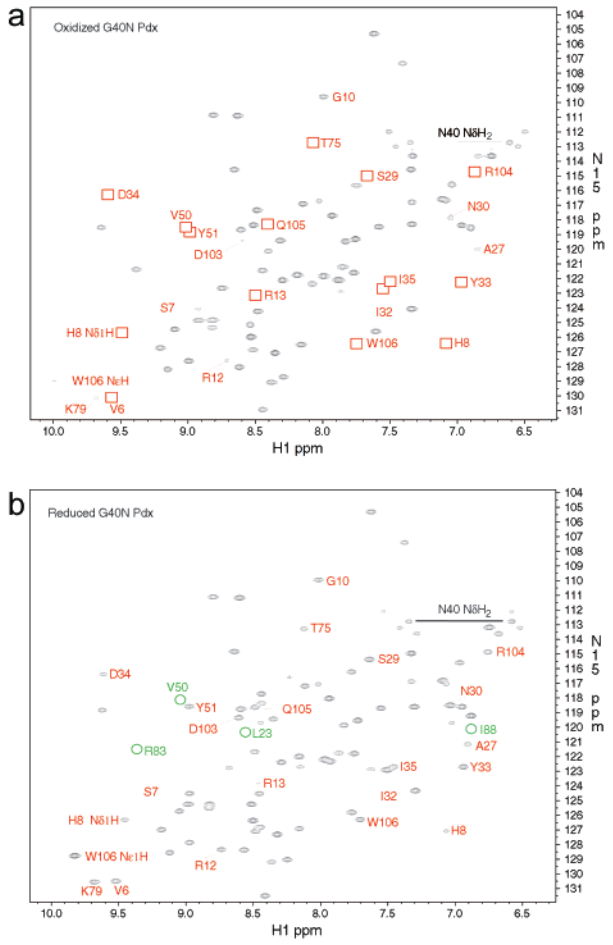

FIGURE 5: 14 T (600 MHz ^{1}H) ^{1}H−^{15}N HSQC spectra of 1 mM G40N Pdx at 290 K and pH 7.4 in 50 mM *d*-Tris-HCl buffer, with a 90/10 H_2O/D_2O mixture: (a) spectrum of G40N Pdx^o and (b) spectrum of G40N Pdx^r. Both spectra were obtained using identical acquisition and processing parameters. The Pdx^o spectrum was obtained first; the sample was then reduced and the Pdx^r spectrum acquired. Both spectra are plotted at a level such that features unaffected by the mutation and change in oxidation state are represented by the same number of contours, but differences between the oxidized and reduced spectra are emphasized. Features labeled in red (marked with boxes in the spectrum of G40N Pdx^o) differ from the corresponding features in WT Pdx^o, but revert to WT patterns in G40N Pdx^r. See the text for details. Features labeled in green (circles on the spectrum of G40N Pdx^r) are lost to paramagnetic broadening in both WT and G40N Pdx^r.

30, Ile 32, Tyr 33, Asp 34, Ile 35, Tyr 51, Thr 75, Lys 79, Asp 103, Arg 104, Gln 105, and Trp 106. Perturbations are also observed at the $N_\delta H$ resonances of His 8 and His 49, as well as the $N_\epsilon H$ signals of Arg 13 and Trp 106. More detailed comparisons of some of the affected resonances between WT and G40N Pdx^o and Pdx^r are shown in Figure 6. In some cases, the affected resonance in G40N Pdx^o is broadened significantly relative to the corresponding resonance in the WT spectrum at the same temperature. For example, the NH resonances of Ser 29, Asp 34, and Arg 104 are broadened to indetectability at 290 K in G40N Pdx^o, but are apparent (although also broadened) in WT Pdx^o at the same temperature. The NH resonances of Ile 32, Tyr 33, and Ile 35 are almost as completely broadened in G40N Pdx^o at 290 K, although inspection of 2D ^{1}H−^{15}N HSQC spectra near the noise shows a complex overlapped series of low-intensity broadened peaks near the normal positions of these resonances in WT Pdx^o (see Figure 6). Smaller but still detectable differences are seen at many of the other resonances listed above (Figure 5), usually as an increased level of broadening of the G40N resonance relative to the corresponding WT resonance.

In a number of cases, peaks are split into groups of relatively well-defined resonances that we interpret as representing conformational substates at slow exchange on the chemical shift time scale (Figures 6 and 7). This is particularly noticeable for the NH resonances of Gly 10 and Thr 75 (Figure 7b). Even in WT Pdx^o, these resonances show evidence of multiplicity (see Figure 7b), suggesting a heirarchy of substates, some of which are at slow exchange only in G40N Pdx^o, and others that are at slow exchange in both the WT and G40N forms at a given temperature. Figure 7a is particularly instructive in this regard. At all three temperatures that are shown (280, 290, and 300 K), the NH resonance of Tyr 33 in WT Pdx^o is observed as a clear singlet with a line width that is relatively unaffected by the temperature changes. In G40N Pdx^o, a very broadened Tyr 33 NH resonance at 280 K broadens to become essentially undetectable at 290 K (although some broad intensity is observed near the noise). At 300 K, a smaller line of low intensity appears near the position of the WT resonance, suggesting that the fast exchange regime is being approached for some subset of the accessible conformational substates. In the same set of spectra, both Ile 32 and Ile 35 undergo similar transformations; narrower, more intense lines are observed in WT than in G40N Pdx^o for both resonances at the same temperatures, indicating faster exchange in WT Pdx^o. Evidence for conformations at slow exchange persists in the G40N Pdx^o spectrum even at 300 K in the form of lower-intensity side peaks apparently associated with both Ile 32 and Ile 35 resonances.

Most remarkably, reduction of G40N Pdx results in the collapse of the broadened and multiplied peaks observed in G40N Pdx^o into peaks with chemical shifts essentially identical to those of WT Pdx^r. We interpret this collapse as an indication that fewer conformational substates are occupied in Pdx^r than in Pdx^o, and that the same states are occupied in both G40N Pdx^r and WT Pdx^r (see Figure 6).

Time Scales of Affected Motions. The temperature dependence of the G40N Pdx^o spectra confirms that the spectral perturbations introduced by the mutation are the result of dynamic processes that are slow to intermediate on the chemical shift time scale (Figures 7 and 8). However, it is important for the conclusions we draw from the G40N mutant to establish that corresponding processes in WT Pdx are faster on the chemical shift time scale. We would expect that such processes might be of the right order of magnitude to contribute to line broadening (i.e., T_2 processes) in WT Pdx^o. Indeed, many of the resonances that show the largest differences between G40N and WT Pdx^o are clearly broadened relative to peaks that are unaffected by the mutation even in WT Pdx^o (see Figure 4). These include the resonances of Tyr 33, Asp 34, Val 50, Arg 104, and Gln 105. To judge the importance of exchange contributions to apparent transverse relaxation rates for different residues, we applied a selection criterion based on the analysis of ^{15}N T_1/T_2 ratios (*32*). If, for a certain residue, the ^{15}N T_1/T_2 ratio is more than one standard deviation above the mean, then it can be assumed that an R_{ex} term must be included in transverse relaxation rate calculations. We determined that

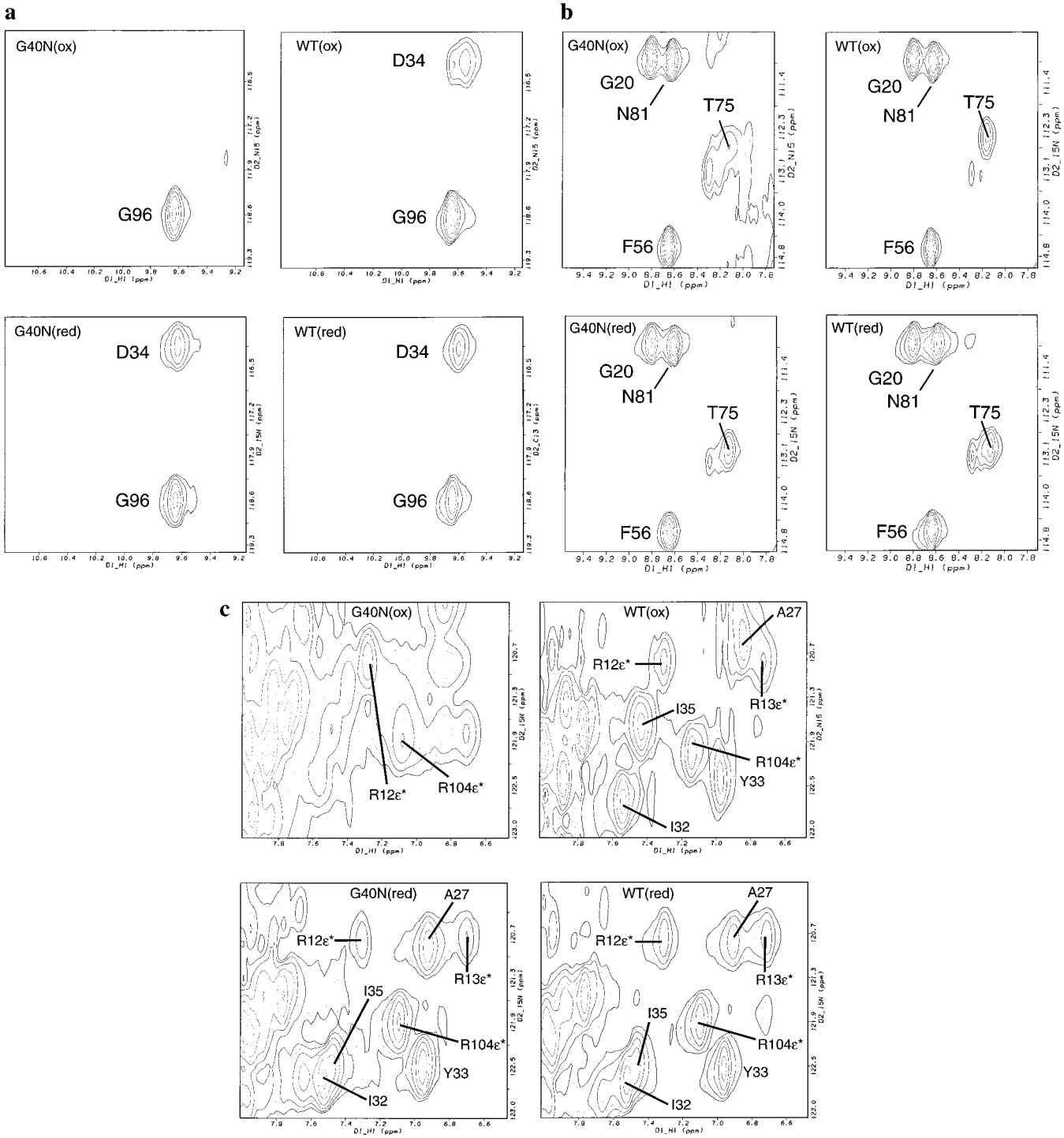

FIGURE 6: Comparison of selected regions of the 11.74 T (500 MHz ^{1}H) ^{1}H−^{15}N HSQC spectra of oxidized and reduced forms of WT and G40N Pdx. Pdx^o and Pdx^r spectra were obtained using the same samples. Pdx^o spectra were obtained first; the samples were reduced, and then the Pdx^r spectra were obtained. All four spectra (WT and G40N Pdx^o and WT and G40N Pdx^r) were obtained and processed using identical acquisition and processing parameters. Samples were at ~1 mM, 290 K, and pH 7.4 in 50 mM *d*-Tris-HCl buffer, with a 90/10 H_2O/D_2O mixture. Spectra are plotted at a level such that reference signals (those unaffected by the mutation and change in oxidation state) are represented by the same number of contours, but differences between the oxidized and reduced spectra are emphasized. Within a block, Pdx^o spectra are shown on top, Pdx^r spectra on the bottom, G40N spectra on the left, and WT spectra on the right. (a) Expansion containing the Asp 34 signal. Gly 96 provides reference. (b) Expansion containing the Thr 75 signal. Phe 56 and Gly 20 provide reference. (c) Expansion containing the Ala 27, Ile 32, Tyr 33, and Ile 35 signals. $N_\epsilon H$ signals of Arg 12 and Arg 104 provide reference (signals are marked with asterisks indicating that they are folded in the ^{15}N dimension from their true resonance frequencies).

residues Val 6, His 8, Arg 12, Tyr 33, Asp 34, and Lys 79 in WT Pdx^o have T_1/T_2 ratios more than one standard deviation above the mean at both 11.74 and 14 T (Figure 9). These results are in agreement with those reported by Sari et al. (*15*) for Pdx^o at 11.74 T. All of these residues are affected by the G40N mutation in Pdx^o, so we assume that the motional behavior responsible for exchange broadening in WT Pdx at these residues corresponds to the same motional behavior observed in a slower exchange regime in the G40N mutant. For these residues, approximate R_{ex} terms,

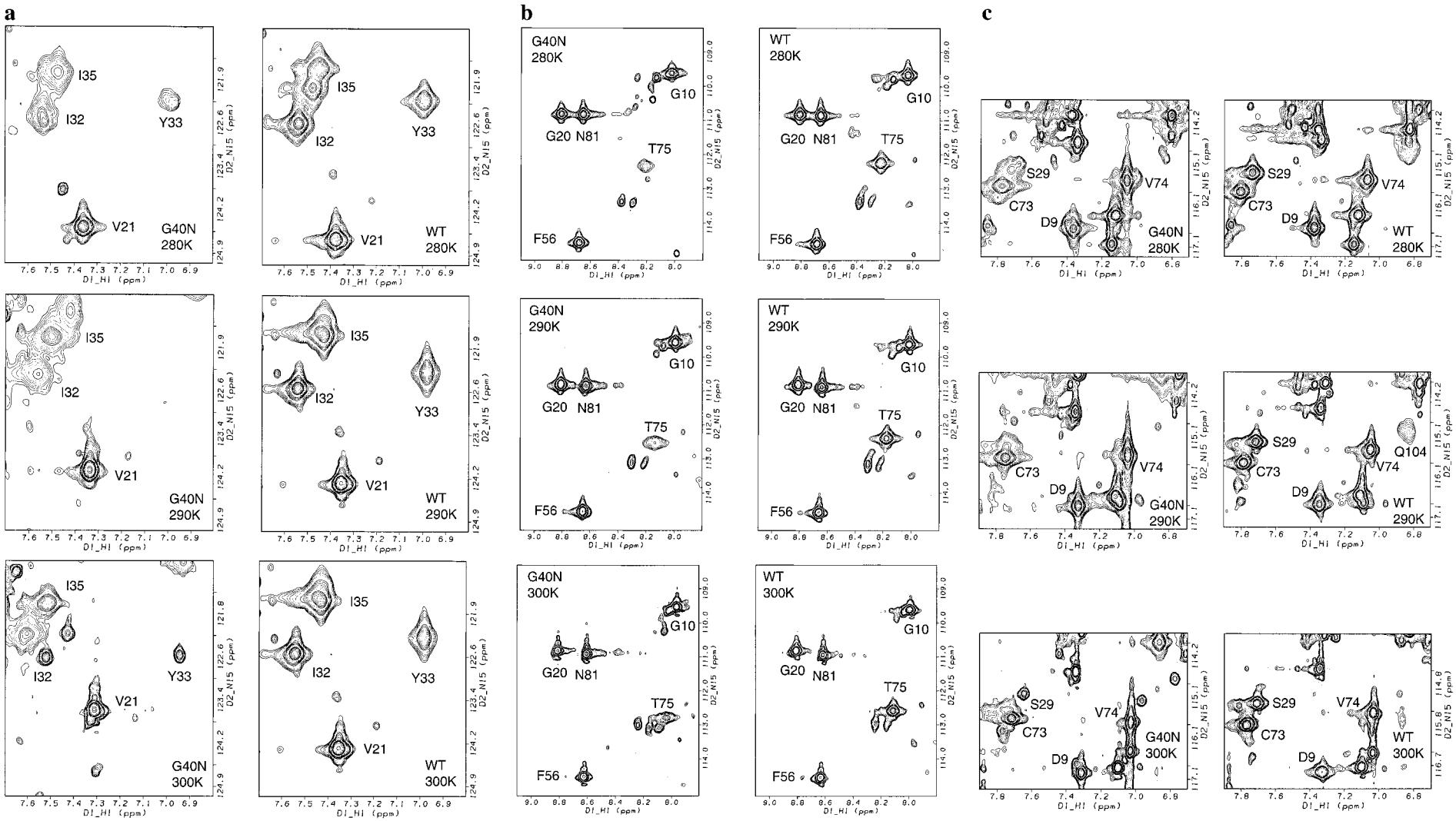

FIGURE 7: Temperature dependence of corresponding regions of high-resolution 14 T (600 MHz ^{1}H) ^{1}H−^{15}N HSQC spectra of WT Pdx^o and G40N Pdx^o. Spectra were obtained at 280, 290, and 300 K. All spectra were obtained and processed using identical acquisition and processing parameters. Sufficient increments were obtained in the ^{15}N dimension to obtain complete ^{15}N T_2* envelopes, thereby maximizing resolution. No linear prediction was used for processing in either dimension. Resolution enhancment was achieved in the ^{1}H dimension using a Gaussian function, and in the in the ^{15}N dimension using an 80° shifted squared sine bell. Both samples were at 1 mM, 290 K, and pH 7.4 in 50 mM *d*-Tris-HCl buffer, with a 90/10 H_2O/D_2O mixture. Spectra are plotted at a level such that reference signals (those unaffected by the mutation and change in oxidation state) are represented by the same number of contours, and that low-intensity features are visible. Within each block, G40N spectra are plotted on the left and WT spectra on the right. The top rank is 280 K, the middle rank 290 K, and the bottom rank 300 K. (a) Expansion containing the Val 21, Ala 27, Ile 32, Tyr 33, and Ile 35 signals. No unaffected signals are visible in the expansion, but reference signals outside the region shown were at similar intensities. (b) Expansion containing the Gly 10 and Thr 75 signals. References are provided by Gly 20, Asn 81, and Phe 56. (c) Expansion containing the Ser 29 and Gln 104 signals. References are provided by Asp 9, Cys 73, and Val 74.

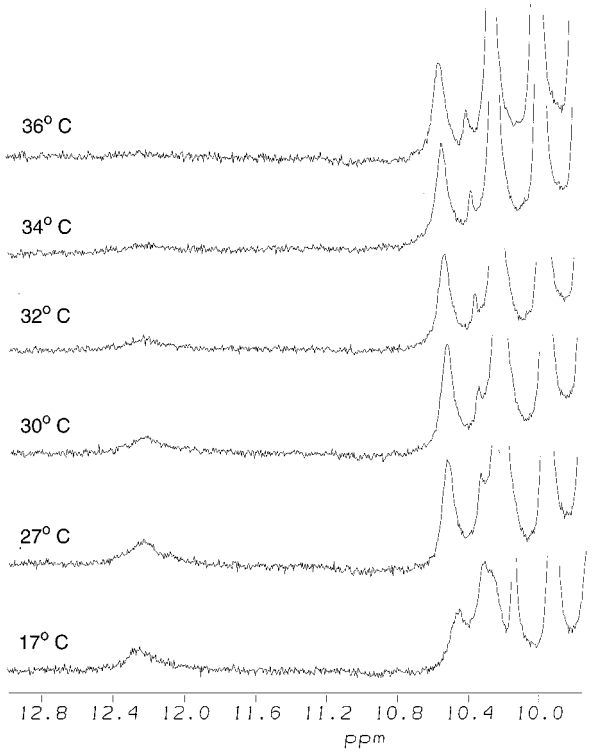

FIGURE 8: Downfield region of the 500 MHz ^{1}H spectrum of G40N Pdx^o shown as a function of temperature. Increased broadening of the His 49 $N_\delta H$ resonance (12.3 ppm) with increasing temperature demonstrates that the processes causing the broadening are slow on the chemical shift time scale. The phenomenon shown is reversible.

for both fields, were calculated by assuming that

$$(1/T_2)_{app} = (1/T_2)_{ave} + R_{ex} \quad (1)$$

where $(1/T_2)_{app}$ is the apparent transverse relaxation rate for a given residue, as calculated from nonlinear curve fitting of relaxation data, and $(1/T_2)_{ave}$ is the average transverse relaxation rate of the neighboring residues that are not affected by chemical exchange (that is, their T_1/T_2 ratios do not differ from the mean by at least one standard deviation unit). The simplifying assumption is made that the transverse relaxation rate of nearby residues is a good approximation of the residue's own transverse relaxation rate in the absence of chemical exchange. The R_{ex} values shown in Table 1 are likely underestimates of the real R_{ex} terms, probably because the "intrinsic" $(1/T_2)_{ave}$ terms used still contain an unidentified exchange contribution as well.

It has recently been pointed out by Millet et al. (*33*) that in cases where exchange is slow on the chemical shift time scale but takes place between sites with very different relative populations, it is possible to mistake the situation for a fast exchange regime. These researchers provide fairly simple criteria for determining whether such a situation exists for the case of slow exchange between two unequally populated sites. They use the static magnetic field dependence of ^{15}N T_1 and T_2 values to examine the exchange contribution to relaxation behavior. In the current case, we are considering a series of conformations linked by exchange, with state populations that may be quite similar across the exchange. As such, we cannot quantitatively evaluate the exchange contribution using the criteria of Millet et al. We note that

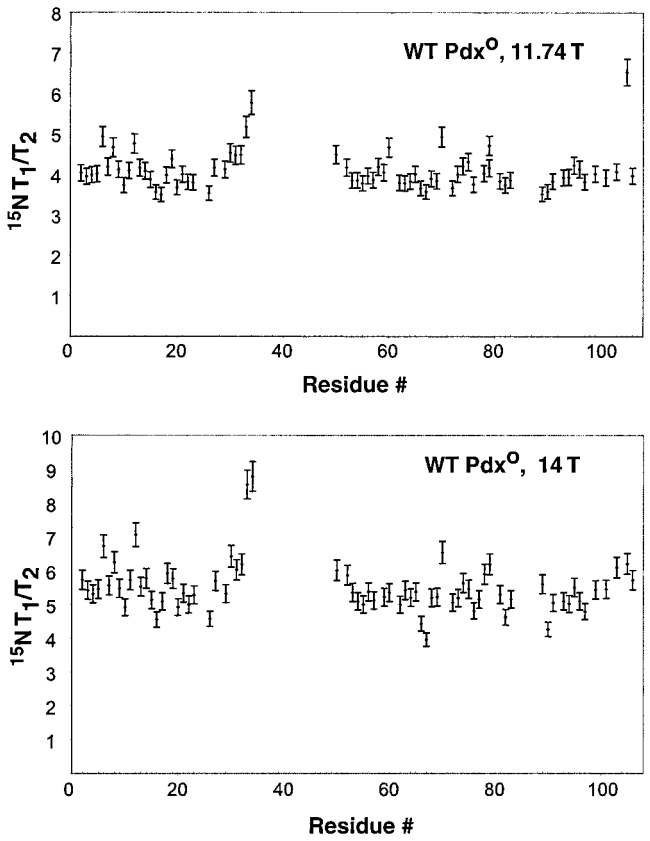

FIGURE 9: ^{15}N T_1/T_2 ratios as a function of magnetic field strength. Measurements were taken on the same sample (1 mM WT Pdx^o, at 290 K and pH 7.4 in 50 mM *d*-Tris-HCl buffer, with a 90/10 H_2O/D_2O mixture) as described in Materials and Methods. Error bars correspond to the percentage error of the T_1/T_2 ratio, calculated as $\Delta(T_1/T_2) = \Delta T_1 + \Delta T_2$, where ΔT_1 and ΔT_2 are taken to be 2.5%, as estimated from repeated measurements (see Materials and Methods for complete description). The field-dependent behavior of residue 105 is reproducible, and could be due to dynamic processes involving the C-terminus of Pdx (see ref *14* for more details).

Table 1: Approximate R_{ex} and α (scaling factor for field dependence for R_{ex} as described in ref *33*) for WT Pdx^o Residues That Exhibit a Significant Chemical Exchange Contribution to ^{15}N Transverse Relaxation Rate, As Indicated by ^{15}N T_1/T_2 Ratios Differing by More Than One Standard Deviation from the Mean at both 11.74 and 14 T (see Figure 9)

residue	R_{ex1} (s^{-1}) (11.74 T)	R_{ex2} (s^{-1}) (14 T)	α
Val 6	1.98	2.54	1.3
His 8	2.44	2.95	1.0
Arg 12	1.87	3.26	2.9
Tyr 33	0.80	2.46	5.5
Asp 34	2.88	6.14	3.9
Lys 79	1.77	2.14	1.0

the scaling factors calculated from our field dependence for R_{ex} are all greater than 1, as expected for the fast exchange regime (*33*). We are currently examining alternative methods for evaluating the true contribution of multisite exchange to observed nuclear relaxation behavior.

DISCUSSION

Metal Cluster Binding Loop of Pdx as the Origin of Redox-Dependent Dynamics. The sites to be mutated in this study were chosen primarily because of their predicted importance in redox-dependent conformational selection in Pdx. It is

Table 2: ^{15}N Chemical Shifts, T_1 Relaxation Times, and Chemical Shift Temperature Dependencies for Residues in the Metal Cluster Binding Site of WT Pdx[a]

residue	T_1 (Pdx^o, Pdx^r) (ms)	^{15}N shift (Pdx^o, Pdx^r) (δ, ppm)	$\Delta\delta$, ΔT (Pdx^o, Pdx^r) (Hz, K)
D38	42, 30	121.7, 120.8	1.9, −0.3
C39	29, 8	107.2,* 182.5*	0.8, −11.2
G40	56, 25	117.6, 124.2	0.6, −1.1
G41	19, 50	156.2, 124.8	6.3, −1.4
S42	47, 12	139.5, 176.6	2.2, −2.6
A43	30, 80	131.0, 120.7	6.7, 0.2
S44	32, 10	132.1, 87.9	5.8, 9.8
C45	22, 9	136.2, 140.8	1.0, −6.6
A46	34, 60	137.5, 121.0	7.2, 0.1
T47	37, 20	146.6, 85.6	5.7, 16.5
C48	58, 4	126.7,* 272.7*	1.9, (−60)*
L84	55, 65	120.6, 122.8	1.3, −5.0
C85	52, 30	135.4, 139.8	1.8, −3.1
C86	37, 2	151.0, 260.5	1.7, (−60)*
Q87	53, 15	129.8, 160.2	1.6, −8.3

[a] Chemical shift assignments were made using selective labeling and double-resonance techniques as reported elsewhere (*22*, *23*). Assignments and values marked with an asterisk are tentative, as described in refs *22* and *23*. All entries are reported as values for WT Pdx^o as the first value and WT Pdx^r as the second.

reasonable to assume that such redox dependence arises primarily within the Fe_2S_2 binding loop. This surface-exposed loop (G_{37}-D_{38}-**C**$_{39}$-G_{40}-G_{42}-S_{42}-A_{43}-S_{44}-**C**$_{45}$-A_{46}-T_{47}-**C**$_{48}$-H_{49}) contains three of the four cysteinyl ligands of the metal cluster (underlined). The amino acid composition of this loop is such that considerable backbone flexibility might be expected. Evidence from a variety of sources suggests that considerable differences in local conformation and dynamics exist between Pdx^o and Pdx^r in this region. First, the largest changes in NMR-accessible protein dynamics occur for residues either sequentially or spatially adjacent to the metal cluster binding loop (*12*, *15*). Second, ^{2}H ESEEM studies of the closely related ferredoxin adrenodoxin (Adx) indicate that H−D exchange within the metal cluster binding loop of that protein is highly redox-dependent. While exchangeable protons near the metal cluster (presumably in the metal cluster binding loop) exchange rapidly with deuterons in the solvent in Adx^o, such exchange is much slower in Adx^r (*34*). Finally, Markley and co-workers report evidence for significant conformational differences in the NMR-accessible regions of Adx homologous to Ser 22 and Leu 23 in Pdx (*35*).

Evidence for Redox-Dependent Conformational Changes from Hyperfine-Shifted ^{15}N and ^{13}C Resonances. Recently, we reported redox-dependent hyperfine shifts and nuclear spin relaxation rates for amide ^{15}N and ^{13}C═O resonances in both oxidation states of Pdx (*22*, *23*). Patterns of hyperfine shifts, temperature effects, and nuclear spin relaxation rates strongly suggest localized redox-dependent conformational changes in the Pdx metal cluster binding loop (Table 2 and Figure 10). The ^{15}N resonances of several residues (Gly 41, Ala 43, and Ala 46) relax more slowly and move toward the diamagnetic region of the spectrum upon reduction. The shifts of these same resonances also show smaller temperature dependencies in Pdx^r than in Pdx^o, evidence for less interaction with unpaired electron spin density. At the same time, the ^{15}N resonances of the adjacent residues (Ser 42, Ser 44, and Thr 47) show marked increases in relaxation rates, significant hyperfine shifts, and increases in temperature sensitivity of chemical shifts in Pdx^r relative to Pdx^o.

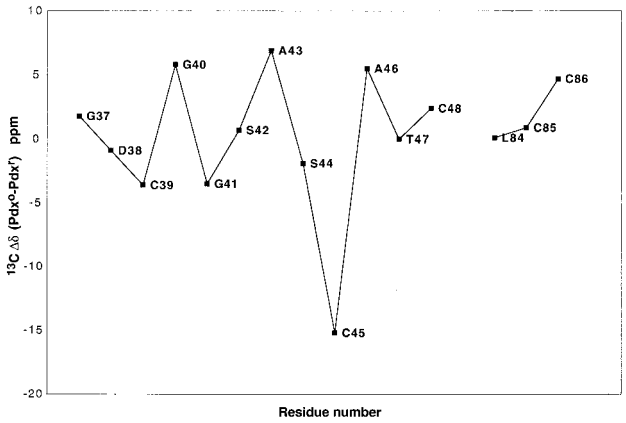

FIGURE 10: Carbonyl ^{13}C chemical shift changes ($\Delta\delta$) in parts per million as a function of oxidation state for residues in the metal binding loop (Gly 37−Cys 48) and Leu 84−Cys 86. Assignments were made as described in refs *22* and *23*.

Taken together, these observations suggest a conformational change that moves the NH groups of Gly 41, Ala 43, and Ala 46 further from the metal cluster upon reduction, while moving the NH groups of Ser 42, Ser 44, and Thr 47 closer. On the basis of comparison with the crystal structure of oxidized adrenodoxin (*36*), the NH protons of Ser 44 and Thr 47 are expected to form hydrogen bonds to the cysteinyl Sγ sulfur atoms ligating Fe_1 of the metal cluster (Cys 39 and Cys 45, respectively). The parallel behavior of the ^{15}N shifts of Ser 44 and Thr 47 upon reduction suggests increased unpaired spin delocalization onto these nitrogens in Pdx^r, presumably via those hydrogen bonds. This could reflect a strengthening of the hydrogen bonds to the cluster from these amides, as expected due to the increased negative charge of the cluster in Pdx^r. A significant shortening of homologous S···HN hydrogen bonds is detected in the X-ray crystal structure of reduced *Anabaena* PCC7119 ferredoxin compared to the structure of the oxidized form (*37*).

Also pertinent are changes in ^{13}C═O shifts within the metal cluster binding region. ^{13}C═O resonances for residues in the loop region also show an alternating pattern in redox-dependent hyperfine shifts (Figure 10). Since carbonyl groups are not implicated in direct interactions with the metal center (such as hydrogen bonding), the changes in ^{13}C═O hyperfine shifts may more so reflect real structural perturbations than changes in unpaired spin density (i.e., changes in through-space interactions with the metal cluster as opposed to through-bond).

We interpret the pattern of redox-dependent changes in amide resonances in the cluster binding loop to mean that, upon reduction, the polypeptide loop from Cys 39 to Ala 46 undergoes an increased "puckering"; that is, the NH groups of Ser 42, Ser 44, and Thr 47 move closer to the metal cluster, while those of Gly 41, Ala 43, and Ala 46 move further away. This puckering would result from the strengthening (shortening) of hydrogen bonds between the metal cluster and the binding loop amides in Pdx^r. Shortening these bonds would result in a contraction of the binding loop around the metal center. The NH groups of Ser 42, Ser 44, and Thr 47 are probably forming hydrogen bonds to the cluster, since these are the residues (along with ligands Cys 39 and Cys 45) for which ^{15}N chemical shifts reflect the largest increases in the level of interaction with the metal center upon reduction. It should be noted that there will be

differential effects in Pdx^r depending on which of the two iron centers most influence a particular spin. Fe(1), which is expected to contain the extra electron gained by reduction (*38*), will give rise to Curie-type behavior, while Fe(2) will give rise to anti-Curie temperature effects (*39*). However, on the basis of structural considerations, the ^{15}N nuclei that are being compared (those of Gly 41, Ser 42, Ala 43, Ser 44, Ala 46, and Thr 47) are all expected to be interacting primarily with Fe(1), so the comparison of redox-dependent changes in ^{15}N resonances is valid within this set.

Roles of Gly 40 and Gly 41 in Local Dynamics. The proposed contraction of the metal binding loop of Pdx upon reduction would require that some portion(s) of the polypeptide be able to take up the slack that contraction would generate in the peptide chain. That portion of the chain should not be critical for ligating or hydrogen bonding to the iron sulfur cluster, and should be without large steric barriers to conformational changes. The adjacent loop residues Gly 40 and Gly 41 fit this description. The lack of side chains and the accessibility of larger allowed regions of Ramachandran space for Gly would ease dihedral rotations for these two residues considerably. Of the two Gly residues, only the ^{15}N resonance of Gly 41 shows evidence of significant interaction with the metal cluster, and then only in Pdx^o (Table 2). In Pdx^r, this resonance moves toward the diamagnetic envelope and shows smaller temperature effects than in Pdx^o. We replaced Gly with Asn in the mutation experiments described here because Asn is the only residue besides Gly that regularly occupies a positive ϕ backbone dihedral angle, and both Gly 40 and Gly 41 are expected to have positive ϕ angles (*10*). We expected that the side chain of Asn would increase the barrier to these hinge motions sufficiently so that they might be considerably slowed in the mutant. At least in the G40N mutant, this appears to be the case.

The decreased stability of the other mutations (G41N, G40N/G41N, and ΔG41) also make sense in terms of the contraction model. The shortened metal cluster binding loop of the deletion mutant, ΔG41, should not be able to accommodate the steric demands of the oxidized metal center while maintaining the expected hydrogen bonding network, and should be less able to stabilize the metal cluster. On the basis of the structure, the side chain of Asn 41 in the G41N and G40N/G41N mutants should interfere sterically with the metal cluster, and so destabilize the formation of the holoprotein.

Coupling of Metal Binding Loop Conformational Changes to the C-Terminal Cluster. One conclusion that can be reached from the NMR data shown here is that the mutations within the metal binding loop clearly affect protein dynamics in adjacent regions of Pdx. Three regions are affected in particular. The first includes the residues immediately preceding the metal binding loop (Asn 30−Ile 35) and residues in contact with them (Val 6, Ser 7, His 8, Gly 10, Ala 27, and Ser 29). The second includes residues near the beginning of the α-helix that contact the metal binding loop near Gly 40 and Gly 41 (Ser 22 and Leu 23). The most far-reaching effects, however, are observed in the C-terminal cluster region. As described elsewhere (*11*, *12*), the C-terminal cluster shows considerable sensitivity to redox changes at the metal cluster in terms of amide proton exchange, and also includes the residues that exhibit the largest chemical shift changes with oxidation state of any diamagnetic resonances in the protein (vide supra). The C-terminal cluster is also extremely sensitive to other perturbations in the metal binding loop, including metal cluster reconstitutions (*40*). The role of His 49 is likely to be critical in transmitting redox effects from the metal site to the C-terminal cluster. His 49 is sequentially adjacent to the third cysteinyl ligand of the Fe_2S_2 cluster in the metal binding loop (Cys 48). The side chain imidazole of His 49 is at the core of a well-defined cluster of residues that include Tyr 51, Val 74, Ala 76, Leu 78, Lys 79, and Ser 82 (Figure 2). The NMR structure of Pdx identifies a number of likely hydrogen bonds within the C-terminal cluster. These form a network involving the phenolic OH of Tyr 51, the imidazole $N_{\epsilon 2}$ of His 49 (which is not protonated), and the OγH of Ser 82. In turn, the well-resolved $N_{\delta 1}H$ proton of His 49 appears to hydrogen bond to a backbone carbonyl (Ala 76). The imidazole of His 49 could act as a mechanical linkage between conformational changes in the metal binding loop and the C-terminal cluster. For example, the proposed contraction of the metal binding loop upon reduction would pull on His 49 and, in turn, on residues to which the His 49 imidazole is hydrogen bonded. This would reduce the amplitude of large-scale motions in the C-terminal cluster region. A similar role has been proposed for the homologous His 56 in bovine Adx (*36*). As expected, mutations of His 49 and Tyr 51 both are destabilizing in Pdx (R. Pejchal, unpublished results). It is interesting that the destabilizing mutations G41N, G40N/G41N, and ΔG41 described in this study all result in a loss of the His 49 $N_{\delta 1}H$ resonance as well, confirming the tight linkage between the metal binding loop and the C-terminal cluster.

CONCLUSIONS

The data presented here provide strong support for the conformational selection model of redox-dependent structure and dynamics of Pdx. The primary effect of the G40N mutation is to increase the potential barriers to interconversion between substates, thereby slowing exchange between conformational substates in G40N Pdx^o relative to WT Pdx^o. The slow interconversion between substates in G40N Pdx results in broadening resonances for affected residues in G40N Pdx^o relative to WT Pdx^o or, when exchange between substates is slow on the chemical shift time scale, splitting of individual resonances into multiple peaks corresponding to the multiple occupied substates (Figure 8). On the basis of the complex nature of the spectral changes observed for some residues as a function of temperature, there appears to be a heirarchy of accessible conformational states in both WT and G40N Pdx^o. Within the heirarchy, there is a range of potential barrier heights such that some interconversion processes are at slow exchange while some are at fast or intermediate exchange on the chemical shift time scale.

The data presented here do not allow us to conclude that equilibrium substate populations are unperturbed in G40N Pdx^o relative to WT. However, it is clear that upon reduction, both G40N and WT Pdx occupy the same subset of conformations, as indicated by their nearly identical $^1H-^{15}N$ HSQC spectra at the same temperatures. If substate populations are perturbed in G40N Pdx^o, this should be reflected in the relative binding constants of G40N Pdx^o and Pdx^r for CYP101 as compared to the ratio of the same binding constants measured for WT Pdx (*6*, *7*). We have

found that G40N Pdx exhibits 50% of the activity of WT Pdx in the standard reconstituted PdR/Pdx/CYP101 assay as measured by NADH consumption (R. Pejchal, unpublished results). However, the Asn 40 side chain projects into the proposed Pdx/CYP101 interfacial region (*41*), so it is unclear from these measurements whether the lower activity of the mutant is due to changes in binding constants or interference with electron transfer or some combination thereof. These effects will need to be examined in more detail before firm conclusions can be reached regarding the effect of the G40N mutation on equilibrium substate populations in Pdx^o.

The current results do allow us to localize elements of redox-dependent changes to specific portions of the metal cluster binding loop. The possibility of redox-dependent conformational changes in metalloproteins is not a new idea (*42*), although significant structural effects have not been observed in most cases (*43*, *44*). However, in every instance of which we are aware, metalloproteins exhibit dynamical differences as a function of oxidation state (*12*, *45*, *46*). Very often (although not exclusively; see ref *47*), the oxidized protein displays larger-amplitude motions than the reduced form. We originally proposed that functional differences between Pdx^o and Pdx^r (e.g., tighter binding of Pdx^r to CYP101) originated from dynamic changes rather than structural ones (a structural entropy model). However, this is too simplistic: changes in the amplitudes of motions by definition imply structural differences, if only in displacements around some average structure. We cannot yet say with certainty whether the structures of Pdx^o and Pdx^r both center on the same average structure and differ only in rms displacements around that mean, or if they have different average structures as well. The effect of dipolar interactions on chemical shift cannot be ruled out even for residues remote from the metal center (*44*). As such, the changes in chemical shift between Pdx^o and Pdx^r cannot be taken as firm evidence for different time average structures. Nevertheless, there is precedent for redox-dependent conformational perturbations in ferredoxins. Morales et al. (*37*) noted that one peptide bond in the iron−sulfur cluster binding loop of *Anabaena* ferredoxin appears to reorient upon reduction so as to allow the amide proton to form an additional hydrogen bond to the metal cluster. It may well be that redox-dependent structural and dynamical behavior such as is observed in Pdx is a fairly typical way of controlling activity as a function of oxidation state in ferredoxins.

ACKNOWLEDGMENT

We thank Dorothee Kern for helpful discussions, Timothy McKee for help with 4-primer mutation methodology, and Melissa Heinsen, Duncan Sousa, and Gina Pagani for access to their mass spectrometry data on the mutants. We thank Dr. Susan Sondej Pochapsky for her implementation of the HSQC-NOESY experiment used in this work.

REFERENCES

1. Berendesen, H. J. C., and Hayward, S. (2000) *Curr. Opin. Struct. Biol. 10*, 165−169.
2. Sutcliffe, M. J., and Scrutton, S. (2000) *Philos. Trans. R. Soc. London, Ser. A 358*, 367−386.
3. Miller, D. W., and Agard, D. A. (1999) *J. Mol. Biol. 286*, 267−278.
4. Mueller, E. J., Loida, P. J., and Sligar, S. G. (1995) in *Cytochrome P450: Structure, Mechanism and Biochemistry* (Ortiz de Montellano, P. R., Ed.) pp 83−124, Plenum Press, New York.
5. Lipscomb, J. D., Sligar, S. G., Namtvedt, M. J., and Gunsalus, I. C. (1976) *J. Biol. Chem. 251*, 1116−1124.
6. Hintz, M. J., Mock, D. M., Peterson, L. L., Tuttle, K., and Peterson, J. A. (1982) *J. Biol. Chem. 257*, 14324−14332.
7. Sligar, S. G., and Gunsalus, I. C. (1976) *Proc. Natl. Acad. Sci. U.S.A. 73*, 1078−1082.
8. Pederson, T. C., Austin, R. H., and Gunsalus, I. C. (1977) in *Microsomes and Drug Oxidations* (Ullrich, V., Ed.) pp 275−283, Pergamon Press, Elmsford, NY.
9. Pochapsky, T. C., Ye, X. M., Ratnaswamy, G., and Lyons, T. A. (1994) *Biochemistry 33*, 6424−6432.
10. Pochapsky, T. C., Jain, N. U., Kuti, M., Lyons, T. A., and Heymont, J. (1999) *Biochemistry 38*, 4681−4690.
11. Pochapsky, T. C., Ratnaswamy, G., and Patera, A. (1994) *Biochemistry 33*, 6433−6441.
12. Lyons, T. C., Ratnaswamy, G., and Pochapsky, T. C. (1996) *Protein Sci. 5*, 627−639.
13. Davies, M. D., and Sligar, S. G. (1992) *Biochemistry 31*, 11383−11389.
14. Stayton, P. S., and Sligar, S. G. (1991) *Biochemistry 30*, 1845−1851.
15. Sari, N., Holden, M. J., Mayhew, M. P., Vilker, V. L., and Coxon, B. (1999) *Biochemistry 38*, 9862−9871.
16. Dangi, B., Blankman, J. I., Miller, C. J., Volkman, B. F., and Guiles, R. D. (1998) *J. Phys. Chem. B 102*, 8201−8208.
17. Kitao, A., Hayward, S., and Go, N. (1998) *Proteins 33*, 496−517.
18. Amadei, A., de Groot, B. L., Ceruso, M.-A., Paci, M., Di Nola, A., and Berendsen, H. J. C. (1999) *Proteins 35*, 283−292.
19. Frauenfelder, H., and McMahon, B. H. (2000) *Ann. Phys. 9*, 655−667.
20. Pochapsky, T. C., Arakaki, T., Jain, N., Kazanis, S., Lyons, T. A., Mo, H., Patera, A., Ratnaswamy, G., and Ye, X. (1997) in *Structure, Motion, Interaction and Expression of Biological Macromolecules*, Vol. 2, pp 79−84, Adenine Press, New York.
21. Reipa, V., Holden, M. J., Mayhew, M. P., and Vilker, V. L. (2000) *Biochim. Biophys. Acta 1459*, 1−9.
22. Jain, N. U., and Pochapsky, T. C. (1998) *J. Am. Chem. Soc. 120*, 12984.
23. Jain, N. U., and Pochapsky, T. C. (1999) *Biochem. Biophys. Res. Commun. 258*, 54−59.
24. Jain, N. U. (2000) Ph.D. Thesis, Brandeis University, Waltham, MA.
25. Bax, A., and Subramanian, S. (1986) *J. Magn. Reson. 67*, 565−569.
26. Cavanaugh, J., Palmer, A. G., Wright, P. E., and Rance, M. (1991) *J. Magn. Reson. 91*, 429−436.
27. Kay, L. E., Keifer, P., and Saarinen, T. (1992) *J. Am. Chem. Soc. 114*, 10663−10665.
28. Shaka, A. J., Barker, P. B., and Freeman, R. (1985) *J. Magn. Reson. 52*, 335−338.
29. Kay, L. E., Nicholson, L. K., Delaglio, F., Bax, A., and Torchia, D. A. (1992) *J. Magn. Reson. 97*, 359.
30. Farrow, N. A., Muhandiram, R., Singer, A. U., Pascale, S. M., Kay, C. M., Gish, C. M., Shoelson, S. E., Pawson, T., Forman-Kay, J. D., and Kay, L. E. (1994) *Biochemistry 33*, 5984−6003.
31. Norwood, T. J., Boyd, J., Heritage, J. E., Soffe, N., and Campbell, I. D. (1990) *J. Magn. Reson. 87*, 488−501.
32. Clore, G. M., Driscoll, P. C., Wingfield, P. T., and Gronenborn, A. M. (1990) *Biochemistry 29*, 7387−7401.
33. Millet, O., Loria, P. J., Kroenke, C. D., Pons, M., and Palmer, A. G,. III (2000) *J. Am. Chem. Soc. 122*, 2867−2877.
34. Orme-Johnson, N. R., Mims, W. B., Orme-Johnson, W. H., Bartsch, R. G., Cusanovich, M. A., and Peisach, J. (1983) *Biochim. Biophys. Acta 748*, 68−72.
35. Xia, B., Volkman, B. F., and Markley, J. L. (1998) *Biochemistry 37*, 3965−3973.

36. Müller, A., Müller, J. J., Muller, Y. A., Uhlmann, H., Bernhardt, R., and Heinemann, U. (1998) *Structure 6*, 269−280.
37. Morales, R., Charon, M. H., Hudry-Clergeon, G., Petillot, Y., Norager, S., Medina, M., and Frey, M. (1999) *Biochemistry 38*, 15764−15773.
38. Dugad, L. B., La Mar, G. N., Banci, L., and Bertini, I. (1990) *Biochemistry 29*, 2263−2271.
39. Dunham, W. R., Palmer, G., Sands, R. H., and Bearden, A. (1971) *Biochim. Biophys. Acta 253*, 511.
40. Kazanis, S., and Pochapsky, T. C. (1997) *J. Biomol. NMR 9*, 337−346.
41. Pochapsky, T. C., Lyons, T. A., Kazanis, S., Arakaki, T., and Ratnaswamy, G. (1996) *Biochimie 78*, 723−733.
42. Trewhella, J., Carlson, V. A. P., Curtis, E. H., and Heidorn, D. B. (1988) *Biochemistry 27*, 1121−1125.
43. Berhuis, A. M., and Brayer, G. D. (1992) *J. Mol. Biol. 223*, 959−976.
44. Wilkins, S. J., Xia, B., Weinhold, F., Markley, J. L., and Westler, W. M. (1998) *J. Am. Chem. Soc. 120*, 4806−4814.
45. Marmorino, J. L., Auld, D. S., Betz, S. F., Doyle, D. F., Young, G. B., and Pielak, G. J. (1993*) Protein Sci. 2*, 1966−1974.
46. Gooley, P. R., Zhao, D., and MacKenzie, N. E. (1991) *J. Biomol. NMR 1*, 145−154.
47. Blanchar, L., Blackledge, M. J., Marion, D., and Guerlesquin, F. (1996) *FEBS Lett. 389*, 203−209.

BI0028845